# High Pressure Spherically Expanding Laminar Flame Speed Measurement with Plasma Affected Data

James Shaffer<sup>1</sup> and Omid Askari.<sup>2</sup>
West Virginia University, Morgantown, WV, 256505, USA

Measurements of a propagating flame are crucial to the understanding and verification of important flame phenomena. Specifically, laminar, unstretched flame speed is employed to describe complex flame behavior such as turbulence or stability. This data is necessary because advanced and more efficient combustion devices operate at these high pressures where this data is less reliable from the onset of flame instabilities. This research aims to develop a new flame speed measurement technique as an improvement over the traditional method. The analysis utilizes a constant pressure technique where the velocity of a spherical flame is visually measured. Flame propagation of stoichiometric flame from 1-6 atm are examined at radius up to 20mm at 300K. The novel analysis method incorporates flame data which is ignition affected to improve the traditional constant pressure methods. This allows for with the inclusion of ultra-small, highly stretched flame radii (0-10 mm). Electrical measurements of the ignition are utilized with a thermodynamic model to predict the velocity and temperature which result from plasma formation. This predicted temperature is used describe the influence ignition has on the flame velocity and is compared to the traditional adiabatic flame propagation over the radius observed. The extrapolated laminar burning speed measurement is found for both traditional and novel methods where the novel method has the benefit of additional, previously unused, flame propagation at the high stretch regime. Additionally, practical information about the plasma morphology, crucial to the experimental application of this method is also discussed.

# I. Introduction

The focus of the present research is to provide the foundation and practical methodology of high-pressure laminar burning speed ( $S_u^0$ ) measurements in an ignition affected spherically expanding flame (SEF). The  $S_u^0$  indicates the rate with which the combustible mixture is consumed by a steady, one-dimensional, planar, stretch-free, adiabatic laminar flame [1,2] and is frequently needed in the assessment of various phenomena such as ignition, quenching, stabilization, turbulent flames, and validation of kinetic models. The operating pressures of advanced combustion devices keep increasing, mainly driven by the need to increase cycle efficiencies and improvements in materials. Such combustion devices require accurate  $S_u^0$  measurements at the relevant high-pressure conditions (i.e., 20-100 atm) where the laminar flame is typically difficult to observe without flame front instabilities (i.e., cell formation) at the typical diagnostic flame radii range (>10 mm) [3].

There are a number of approaches for measuring  $S_u^0$ . Among those, the SEF methods are very well-known and widely utilized at pressures well above atmospheric. This approach itself is divided mainly into two different methods: (1) constant volume method [4–6], and (2) constant pressure method [7–9]. In  $S_u^0$  measurement in SEF experiments, having a smooth and spherical flame is key. In order to obtain  $S_u^0$  using the constant volume (CV) method, the flame radius should be large enough, e.g.  $r_f > 0.3 r_{ch}$ , where the pressure inside the combustion chamber starts to increase. However, this method is vulnerable to high initial pressures [10–12] at which the flame becomes unstable due to the

<sup>&</sup>lt;sup>1</sup> PhD Candidate, Mechanical and Aerospace Engineering Department.

<sup>&</sup>lt;sup>2</sup> Associate Professor, Mechanical and Aerospace Engineering Department.

high Peclet number (flame radius to flame thickness ratio). Any perturbation can easily grow and render the flame wrinkled and cellular.

In the second method,  $S_u^0$  is measured by directly imaging the propagating flame front in a constant pressure region which is called hereafter as the conventional constant pressure (CCP) method. In this method, the stretch effect should be subtracted through extrapolation techniques to find the zero-stretch flame speed. In all previous studies using the CCP method, the measurements were restricted to the flames with a radius above  $\sim$ 6-10 mm to avoid spark influences (highly dependent on ignition system design). The problem apparent with the CCP method at high pressures is that there are less or even no sufficient data point from a smooth flame for zero-stretch extrapolation.

The Plasma Constant Pressure, PCP It is well-known that the flame kernel in this region, because of the very small radius, is more resistant to instabilities and remains smooth even for higher initial pressures. This is a result of higher stretch rates and smaller Peclet numbers compared with the CCP method. This early flame data is neglected in the CCP method, due to complexities associated with the modeling of plasma and the energy losses. The fundamental process occurring during the first few milliseconds of experimentation at these small radii is the electrical ignition spark which affects the propagation rate of the flame. However, unlike the flame surface instabilities, this process occurs independent of flame resulting in a separate measurable process that can be accounted for in the analysis. With the careful measurement of the spark discharge processes, the ignition kernel can be experimentally quantified and modeled to extract the additional information of flame propagation during and immediately after the ignition process. The inclusion of this data extends the useful data range for the measurement of  $S_u^0$ . Data presented in this work does not immediately consider the high-pressure data desired but explores a well-understood methane-air initial pressure regime (up to 6 atm) to examine the methodologies and to show the efficacy of the PCP method.

# **II. Model Description**

The PCP model considers the observed early kernel propagation to be the summation of the overall ignition and flame velocity contributions such that  $\dot{r}_f + \dot{r}_p = \dot{r}_b$ . Where r is the radius, f is the flame contribution, p is the ignition plasma contribution, and b is the experimentally observed burned region. The model is derived from first law energy balance and the ideal gas equation such that the relative contribution of both phenomena is shown in Eqs. (1) and (2).  $T_b$  Is the average kernel temperature,  $c_p$  is the specific heat, R is the gas constant,  $\dot{Q}_{net}$  is the net energy supplied to the kernel after losses are considered, A is the kernel surface area, h is the enthalpy,  $\dot{m}$  is the gained mass,  $\rho$  is the density, and  $\Omega$  is the change in the gas constant with respect to temperature. All properties are calculated in Askari [13]

$$\dot{r}_p = \left(\frac{1}{T_b c_{pb}} + \frac{\Omega_b}{R_b c_{pb}}\right) \frac{\dot{Q}_{net}}{\rho_b A_b} + \left[ \left(\frac{1}{T_b c_{pb}} + \frac{\Omega_b}{R_b c_{pb}}\right) (h_u - h_b) + 1 \right] \frac{\dot{m}_p}{\rho_b A_b} \tag{1}$$

$$\dot{r}_f = \left[ \left( \frac{1}{T_b c_{pb}} + \frac{\Omega_b}{R_b c_{pb}} \right) (h_u - h_b) + 1 \right] \frac{\dot{m}_f}{\rho_b A_b} \tag{2}$$

 $\dot{Q}_{net}$ , defined in Eq. (3), is based in experiment where  $V_{gap}$  is the voltage measured across the spark gap (excluding circuit losses) and I is the Current through the spark measured after the spark gap.  $V_{fall}$  is the voltage drop across the plasma sheath (considered to be a non-thermal loss). In this work, this is an unknown parameter solved when fitting the overall data. Two forms of plasma are observed, Arc and Glow discharge, which each have their own characteristic loss. The loss from Glow discharge is on the order of 200-300 V and is dependent on many parameters including the magnitude of current discharge. Arc discharge has a loss on the order of 10-60V. The loss is considered consider constant for the duration of the spark and in previous research has been measured. The measurement of the plasma losses for experiments including flame is challenging, as a result this value is found by fitting parameter along with the Markstein length and the unstretched flame speed. Conduction to the electrode  $\dot{Q}_{cond}$  and radiation losses  $\dot{Q}_{rad}$  are considered, but, observed to be small compared to the overall ignition energy.

$$\dot{Q}_{net} = \left(V_{gap} - V_{fall}\right) * I - \dot{Q}_{cond} - \dot{Q}_{rad} \tag{3}$$

The temperature of the overall kernel can be found using Eq (4), where the kernel gains mass through both flame propagation and kernel effects. The kernel is effectively cooled through these mass gain mechanisms and the kernel is heated by the net ignition power.

$$\dot{T}_b = \frac{\dot{Q}_{net} - (h_b - h_u)\dot{m}_f - (h_b - h_u)\dot{m}_p}{m_b c_{pb}} \tag{4}$$

The mass gain of the kernel because of flame propagation is described using Markstein's curvature-based model to describe the propagation rate of the flame shown in Eq. (5) and (7)

$$\dot{m}_f = S_b^0 \left[ 1 - \frac{2L_b}{r_b} \right] * A_b * \rho_f \tag{5}$$

The growth of the kernel resulting from ignition is attributed to thermal conduction. Eq. (6) relates the Fourier's conduction to the energy added by the mass gained at the properties entering the ignition region. Given the model is zero-dimensional, conduction is approximated using a linear temperature profile in the region directly affected from plasma,  $r_{pl}$  (Eq. (1)). The location of the average temperature in a sphere with a radially linear temperature profile is  $1/4^{th}$  the radius. The properties of the mass which enter the plasma kernel are at the properties of the burnt mixture. At the start of the model (immediately following breakdown), it is assumed that  $r_{pl} \approx r_b$  such that the integration of Eq. (1) is the total plasma effected region without flame.

$$\dot{m}_p = \frac{A_{pl}k \frac{T_b - T_f}{1/4 \, r_{pl}}}{h_f} \tag{6}$$

The traditional laminar burn speed measurement considers only the stretch extrapolation for radii larger after ignition effects are competed. While the scope of this work does not include a detailed comparison of available extrapolation equations, many methods proposed in literature were examined. Markstein's [14]original equation based on curvature was observed to best fit the flame propagation over the largest radius and is shown in Eq. (7) (adjusted for spherically expanding flame to match modern conventions). Here,  $S_b$ , is the flame speed as a function of the radius and,  $S_b^0$ , is the burned gas velocity at zero stretch with  $L_b$ , the Markstein length, being the characteristic thickness of the flame region.

$$S_b = S_b^0 \left[ 1 - \frac{2L_b}{r_b} \right] \tag{7}$$

Of the flame models considered, two prevalent methods based on the stretch are shown in Fig. 1 in justification of the curvature model. Based on the range of data observed in this work, curvature is shown to provide best agreement. The linear model, based on stretch, forces the flame to exist at all radii which is not the case given real flames have minimum quenching sizes. The other equation a nonlinear model proposed by Kelley [15], reduces the velocity of highly stretched flames, but it should be noted that continuing the non-linear expansion to even higher terms shows that this would approximate the curvature-based equation.

For the following results, the data will still be plotted against "stretch" where the axis includes the extrapolated propagation speed,  $K = 2S_b^0/r_b$ . The units work out to stretch and represent the global stretch compared to the planar flame. Note, this work considered stoichiometric conditions however a sample of a rich mixture is shown in Fig. 1 to better indicate the discrepancy between methods.

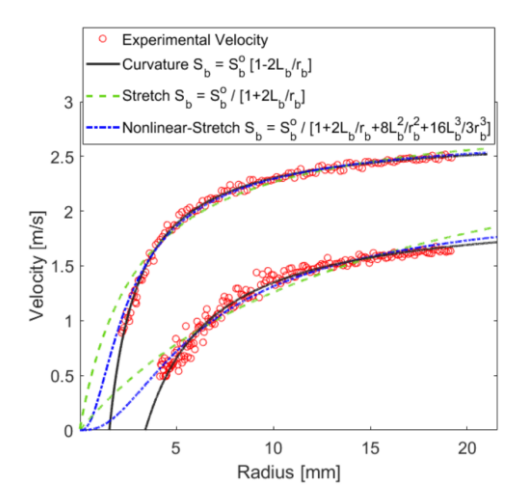


Fig. 1 Comparison of some extrapolation methods, 1atm 300K at 1  $\phi$  (upper curve) and 1.3  $\phi$  (lower curve)

## III. Setup

Experiments are conducted using a constant volume combustion chamber (CVCC) shown in Fig. 2. The CVCC has an internal volume with a diameter and height of 13.3 cm and uses polished quartz disks on either end to provide optical access to the ignition kernel. The experimental diagnostic includes a linear Toepler-type Schlieren system The light source is a red 625 nm Thorlabs led (model M625L4), which is collected with an initial lens (Lens 1) and focused through a 1 mm diameter pinhole to remove excess stray light and make the light as close to a uniform point source as possible. After the pinhole, a plano-convex lens (Lens 2), with a 40 cm focal length, is used to pass collimated light through the plasma discharge, and another plano-convex lens (Lens 3), having a 20 cm focal length, for converging the light over the camera sensor. The Photron FASTCAM SA-Z high-speed camera is utilized to take images during the plasma formation (15,000 fps at 640×640-pixel resolution).

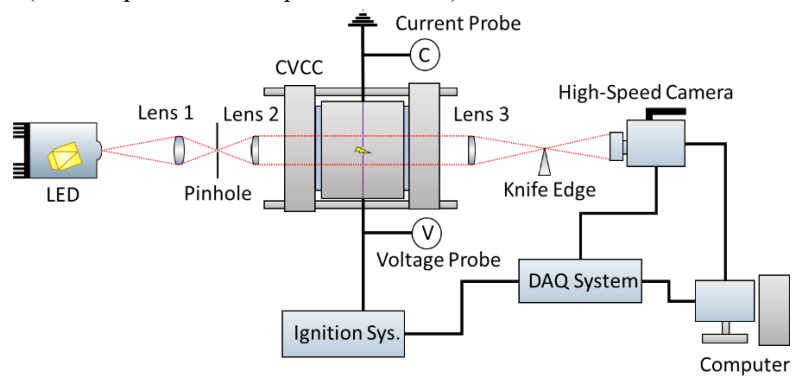


Fig. 2 Diagram of Experimental System.

The ignition system utilizes a  $150 \ uF$  capacitor and a 100:1 automotive ignition coil to provide variable spark energies to the experiment. Glow and Arc discharges with varying intensities are possible over the observed pressure range. The electrodes are  $0.5 \ mm$  stainless steel wire which have been polished using  $5000 \ Grit$  sandpaper. The gap is selected to be small, at around  $0.2 \ mm$  to minimize the effect of breakdown on the results. The results are captured at room temperature of  $300 \ K$ .

# IV. Results

#### A. Preliminary Investigation

Before application of the model, it is important to characterize the effects of both the ignition plasma and flame on the overall data. The best way to do this is observe varying ignition energies versus the kernel size. Since the flame speed is expected to be a function of radius, data which is unaffected by ignition will be shown to over-lap all other experimental data at the same conditions. Flame propagation at stoichiometric atmospheric condition is shown in Fig. 3.

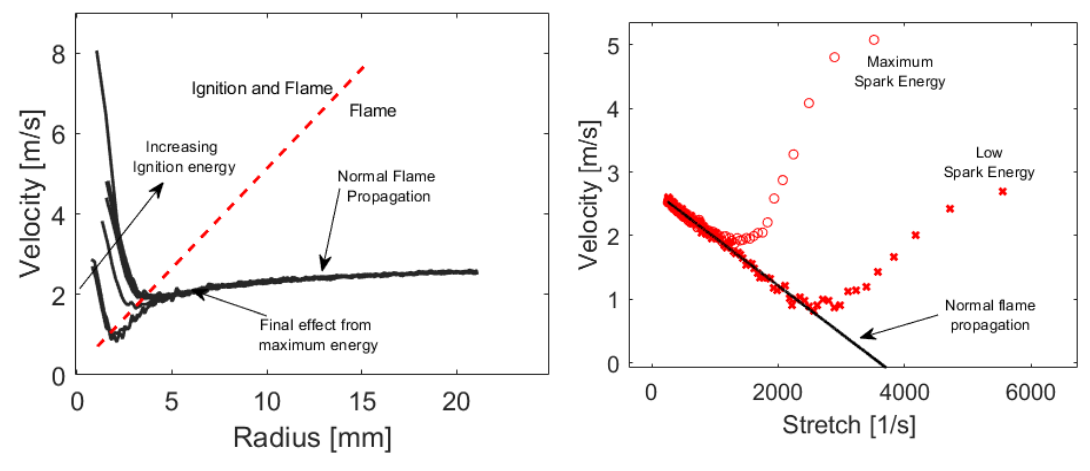


Fig. 3 Experimental propagation data at 1 atm vs Radius (left) and Stretch (right)

It should be noted that even for low energy spark discharge, where flame at small radius (~3-5mm) becomes available, the data continues to fit the linear curvature-based extrapolation. This is the case for glow discharge where the discharge uniform and symmetric. In the case of arc discharge, non-ideal early kernel morphologies are possible which will cause the early radius flame data to deviate (through additional local curvature effects on the flame). After some time, the additional curvature added to the early kernel will be removed through thermal diffusive stabilization resulting in more uniform spherical propagation.

#### **B.** Conventional Measurement

The data and fit of the CCP method are shown in Fig. 4 with numerical results in Table 1. As pressure increases it is expected for the velocity and Markstein length (slope) to decrease. The characteristic length scales of the flame system reduce such that the time for the flame to become similar to the unstretched planar flame is reduced causing the Markstein length to approach zero.

Good agreement was observed with the linear extrapolation however at higher pressure such as 5 and 6 atm the data is seen to wander to some degree about the fit. This is hypothesized to be a result of non-ideal geometries causing some variation the flame curvature resulting in this discrepancy. It is suggested that better control over the flame initiation can be achieved to find better idealized flame propagation and improved flame data than seen here. Given the somewhat random nature of spark ignition this can be challenging to accomplish as pressure increases.

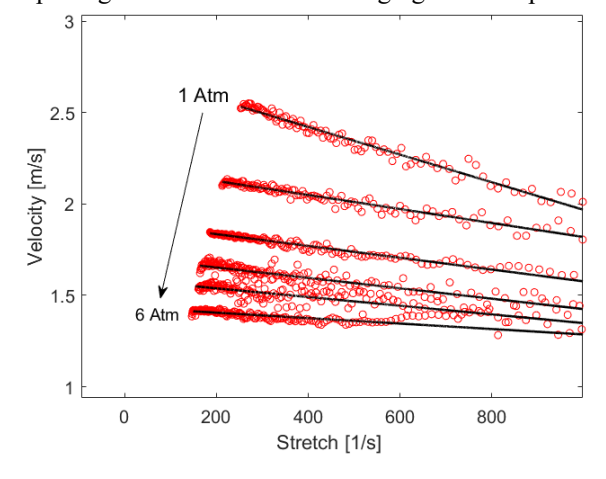


Fig. 4. Extrapolation for stoichiometric methane air conditions 1-6 atm 300K

# C. Novel Approach

The PCP model which includes the effects of ignition are shown in Fig. 5 for stoichiometric flame at 1 atm and at two different ignition energies. Both conditions occurred with pure glow discharge. The effect of each model term on the overall fit is shown. Radiation has a negligible effect given the only the slight increase in temperature (at least 6000K is required). The discharge energy is observed to be significant for up to 5 mm as expected. The Discharge itself is the result of two effects, thermal expansion of the plasma region and mass gain through conduction, the results of the model show the condition through the gas is the most significant compared to the thermal effects (although these are not insignificant themselves).

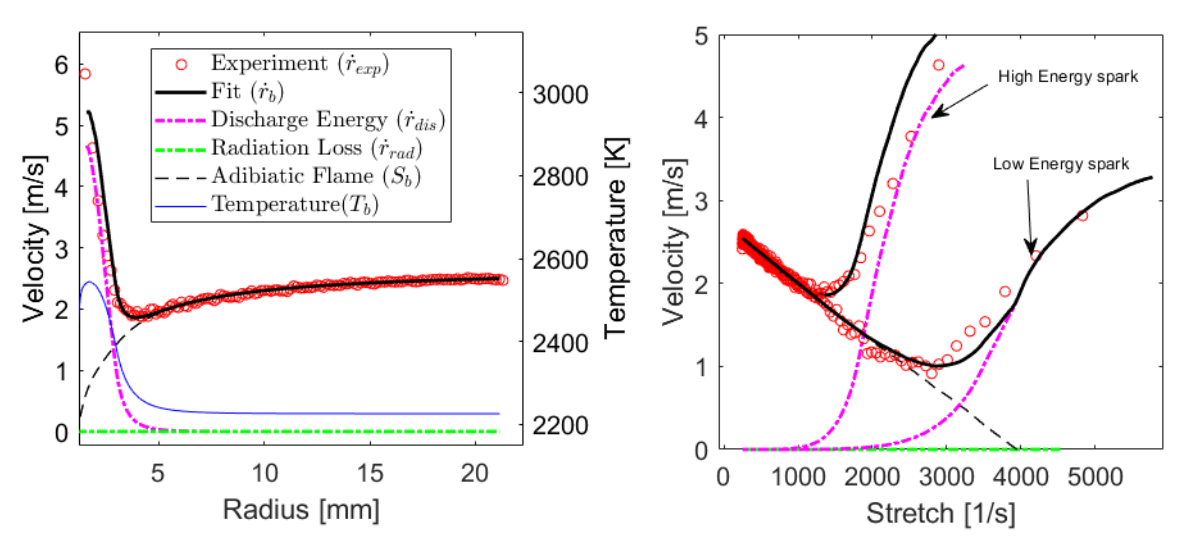


Fig. 5 Model results at 1 atm on a plot of radius (showing high energy spark with temperature) (left) and stretch (right)

The ignition event occurs for a duration of 0.7 ms in all cases. For the low energy spark data in Fig. 5 the flame is shown to only initiated after a significant duration of the spark. This is a result of flame requiring a minimum size to exist, where ignition depend on the amount of energy that reaches this minimum size. Given the fact that ignition can manifest is different plasma types with varying efficiencies, concepts such a minimum ignition energy can be challenging to quantify. Visualization of the spark and flame energy on the stretch plot can help provide insight to the minimum flame geometry and the quenching stretch rate for a self-sustained flame. On the other hand, the high energy spark is shown to exist in tandem with the spark discharge for most of the spark duration.

Arguably better agreement is found for the low energy spark where the shape of the ignition region better matches. Plasma losses were assumed constant over the ignition duration. For the experimental ignition system used in this work, this assumption may become less accurate as ignition energies increase and is something planned to explore in future research.

Model results at 3 atm are shown in Fig. 6. This experiment represents a case of pure arc discharge which is significantly more challenging to achieve and measure accurate result for early flame. The arc discharge is significantly more efficient than glow discharge however the radius it achieves is often far smaller which allows early flame propagation to be visible (potentially beneficial at high pressure).

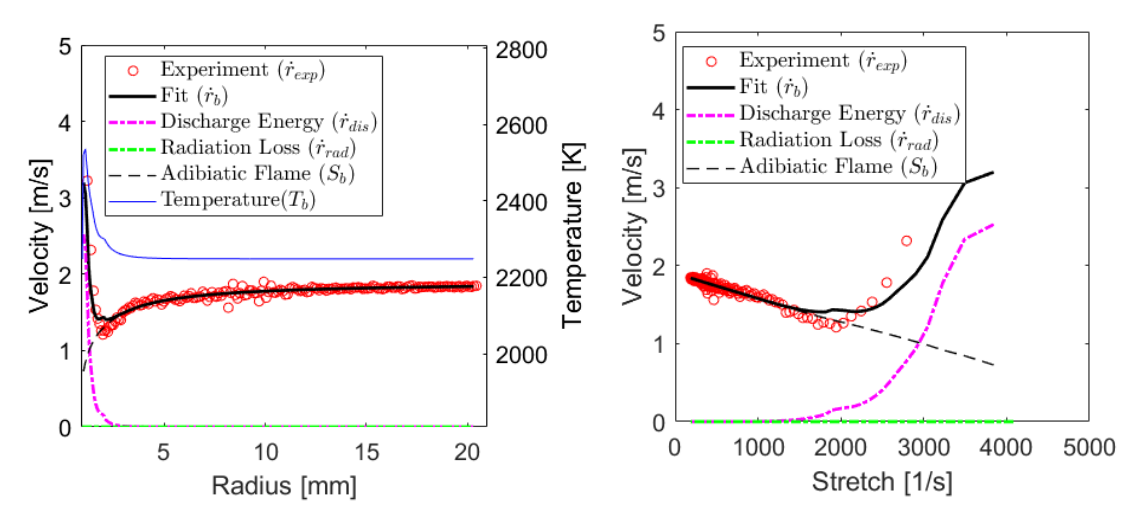


Fig. 6. Model results at 3 atm on a plot of radius (left) and stretch (right)

Arc discharge does not necessarily produce symmetric flame which is especially noticeable at small radius. The propagation at 1000-2000 **1**/s range is observed to be shifted relative to the projected flame extrapolation; this is likely because the small kernel was affected by surface roughness from the arc discharge (which is stabilized at larger radius) but this early kernel was still observed to have a nearly spherical shape. This would suggest that the effective curvature at this time should be greater than expected but these affects are not accounted for in this modeling.

#### D. Comparison to Literature

All results are listed in Table 1. The output of both methods are similar which is expected as there is significant overlap in the measured data.  $L_b$  which notably has high uncertainty is seen to decrease smoothly with pressure for the CCP results. some discrepancy is seen in Markstein length with the full PCP model which is expected to be a result on non-ideal flame geometries at small radii.

**Table 1. All Extrapolation Results** 

		ССР		PCP	
$P_o$	$\rho_u/\rho_b$	$S_u^o$ [cm/s]	$L_b[mm]$	$S_u^o$ [cm/s]	$L_b[mm]$
1 atm	7.47	$35.8 \pm 1.5$	$0.71 \pm 0.1$	$35.8 \pm 1.5$	$0.70 \pm 0.1$
2 atm	7.51	$29.3 \pm 1.4$	$0.40 \pm 0.1$	$29.2 \pm 1.4$	$0.48 \pm 0.1$
3 atm	7.53	$25.1 \pm 1.0$	$0.30 \pm 0.1$	$25.2 \pm 1.0$	$0.32 \pm 0.1$
4 atm	7.55	$22.7 \pm 0.9$	$0.29 \pm 0.1$	$23.3 \pm 0.9$	$0.41 \pm 0.1$
5 atm	7.56	$21.1 \pm 0.9$	$0.26 \pm 0.1$	$21.1 \pm 0.9$	$0.26 \pm 0.1$
6 atm	7.57	$19.2 \pm 0.8$	$0.21 \pm 0.1$	$19.2 \pm 0.8$	$0.18 \pm 0.1$

The  $S_u^o$  obtained using both PCP and CCP methods in this work have been compared to available experimental [7,16–24] data in the literature and the calculated ones via different chemical mechanisms [25–28] shown in Fig. 7. Our measurement shows a good agreement with other data for all pressures. Additionally, the  $S_u^o$  calculated with the CCP method produce a similar curve profile as PCP one, which proves the reproducibility of the PCP method.

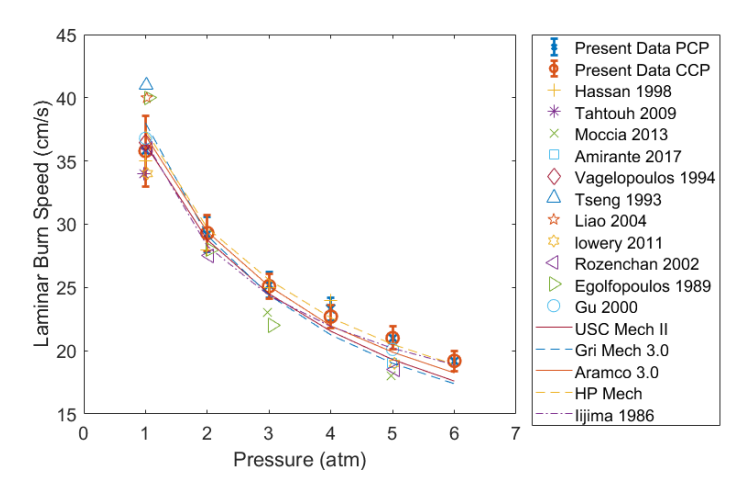


Fig. 7. Comparison to literature.

### V. Conclusion

A novel approach has been presented for flame speed measurements with data presented for 1-6 atm of stochiometric methane air combustion. A good agreement between the experimental data and the proposed model has been shown and agrees with literature. Future research will require higher resolution early flame data to better describe and understand the combined flame and ignition plasma system. As well as further details regarding the plasma loss mechanisms to improve agreement during the ignition phase. The study of the ignition process also provides insight as to the extent which flame data is affected even after the ignition has ended. With further improvements, the inclusion of this ignition data should reduce the necessary upper data range required extending the range of measurement to flames with greater pressure and buoyancy.

#### Acknowledgments

Support from the National Science Foundation under Federal Award No. CBET-2039486 issued through Combustion and Fire System program (John Daily, Program Manager) is greatly appreciated.

#### References

- [1] Law, C. K., 1989, "Dynamics of Stretched Flames," Symp. Combust., 22(1), pp. 1381–1402. DOI 10.1016/S0082-0784(89)80149-3.
- [2] Law, C. K., and Sung, C. J., 2000, "Structure, Aerodynamics, and Geometry of Premixed Flamelets," Prog. Energy Combust. Sci., 26(4), pp. 459–505. DOI 10.1016/S0360-1285(00)00018-6.
- [3] Essmann, S., Markus, D., Grosshans, H., and Maas, U., 2020, "Experimental Investigation of the Stochastic Early Flame Propagation after Ignition by a Low-Energy Electrical Discharge," Combust. Flame, **211**, pp. 44–53. DOI 10.1016/j.combustflame.2019.09.021.
- [4] Lewis, B., and Von Elbe, G., 1987, "Combustion, Flames, and Explosions of Gases," p. 739.
- [5] Metghalchi, M., and Keck, J. C., 1982, "Burning Velocities of Mixtures of Air with Methanol, Isooctane, and Indolene at High Pressure and Temperature," Combust. Flame, **48**(C), pp. 191–210. DOI 10.1016/0010-2180(82)90127-4.
- [6] Askari, O., Moghaddas, A., Alholm, A., Vien, K., Alhazmi, B., and Metghalchi, H., 2016, "Laminar Burning Speed Measurement and Flame Instability Study of H2/CO/Air Mixtures at High Temperatures and Pressures Using a Novel Multi-Shell Model," Combust. Flame. DOI 10.1016/j.combustflame.2016.03.018.
- [7] Rozenchan, G., Zhu, D. L., Law, C. K., and Tse, S. D., 2002, "Outward Propagation, Burning Velocities, and Chemical Effects of Methane Flames up to 60 ATM," Proc. Combust. Inst., **29**(2), pp. 1461–1470. DOI https://doi.org/10.1016/S1540-7489(02)80179-1.
- [8] Donohoe, N., Heufer, A., Metcalfe, W. K., Curran, H. J., Davis, M. L., Mathieu, O., Plichta, D., Morones, A., Petersen, E. L., and Güthe, F., 2014, "Ignition Delay Times, Laminar Flame Speeds, and Mechanism Validation for Natural Gas/Hydrogen Blends at Elevated Pressures," Combust. Flame, **161**(6), pp. 1432–1443.

- DOI https://doi.org/10.1016/j.combustflame.2013.12.005.
- [9] Bradley, D., Gaskell, P. H., and Gu, X. J., 1996, "Burning Velocities, Markstein Lengths, and Flame Quenching for Spherical Methane-Air Flames: A Computational Study," Combust. Flame, **104**(1–2), pp. 176–198. DOI 10.1016/0010-2180(95)00115-8.
- [10] Zare, S., Roy, S., El Maadi, A., and Askari, O., 2019, "An Investigation on Laminar Burning Speed and Flame Structure of Anisole-Air Mixture," Fuel, **244**, pp. 120–131. DOI 10.1016/j.fuel.2019.01.149.
- [11] Askari, O., Wang, Z., Vien, K., Sirio, M., and Metghalchi, H., 2017, "On the Flame Stability and Laminar Burning Speeds of Syngas/O2/He Premixed Flame," Fuel, **190**, pp. 90–103. DOI 10.1016/j.fuel.2016.11.042.
- [12] Askari, O., Vien, K., Wang, Z., Sirio, M., and Metghalchi, H., 2016, "Exhaust Gas Recirculation Effects on Flame Structure and Laminar Burning Speeds of H2/CO/Air Flames at High Pressures and Temperatures," Appl. Energy, 179(C), pp. 451–462. DOI 10.1016/J.APENERGY.2016.06.118.
- [13] Askari, O., 2018, "Thermodynamic Properties of Pure and Mixed Thermal Plasmas Over a Wide Range of Temperature and Pressure," J. Energy Resour. Technol. Trans. ASME, **140**(3). DOI 10.1115/1.4037688.
- [14] MARKSTEIN, G. H., 1988, "Experimental and Theoretical Studies of Flame-Front Stability," *Dynamics of Curved Fronts*, Academic Press, pp. 413–423.
- [15] Kelley, A. P., Bechtold, J. K., and Law, C. K., 2012, "Premixed Flame Propagation in a Confining Vessel with Weak Pressure Rise," J. Fluid Mech., 691, pp. 26–51. DOI 10.1017/jfm.2011.439.
- [16] Hassan, M. I., Aung, K. T., and Faeth, G. M., 1998, "Measured and Predicted Properties of Laminar Premixed Methane/Air Flames at Various Pressures," Combust. Flame, 115(4), pp. 539–550. DOI 10.1016/S0010-2180(98)00025-X.
- [17] Moccia, V., and D'Alessio, J., 2013, "Burning Behaviour of High-Pressure CH4-H2-Air Mixtures," Energies, **6**(1), pp. 97–116. DOI 10.3390/en6010097.
- [18] Amirante, R., Distaso, E., Tamburrano, P., and Reitz, R. D., 2017, "Laminar Flame Speed Correlations for Methane, Ethane, Propane and Their Mixtures, and Natural Gas and Gasoline for Spark-Ignition Engine Simulations," Int. J. Engine Res., **18**(9), pp. 951–970. DOI 10.1177/1468087417720018.
- [19] Liao, S. Y., Jiang, D. M., Gao, J., and Huang, Z. H., 2004, "Measurements of Markstein Numbers and Laminar Burning Velocities for Natural Gas-Air Mixtures," Energy and Fuels, **18**(2), pp. 316–326. DOI 10.1021/EF034036Z.
- [20] Lowry, W., De Vries, J., Krejci, M., Petersen, E., Serinyel, Z., Metcalfe, W., Curran, H., and Bourque, G., 2011, "Laminar Flame Speed Measurements and Modeling of Pure Alkanes and Alkane Blends at Elevated Pressures," J. Eng. Gas Turbines Power, 133(9). DOI 10.1115/1.4002809/409254.
- [21] Egolfopoulos, F. N., Cho, P., and Law, C. K., 1989, "Laminar Flame Speeds of Methane-Air Mixtures under Reduced and Elevated Pressures," Combust. Flame, 76(3–4), pp. 375–391. DOI 10.1016/0010-2180(89)90119-3.
- [22] Gu, X. J., Haq, M. Z., Lawes, M., and Woolley, R., 2000, "Laminar Burning Velocity and Markstein Lengths of Methane–Air Mixtures," Combust. Flame, 121(1–2), pp. 41–58. DOI 10.1016/S0010-2180(99)00142-X.
- [23] Stone, R., Clarke, A., and Beckwith, P., 1998, "Correlations for the Laminar-Burning Velocity of Methane/ Diluent/Air Mixtures Obtained in Free-Fall Experiments."
- [24] Han, P., David Checkel, M., Fleck, B. A., and Nowicki, N. L., 2006, "Burning Velocity of Methane/Diluent Mixture with Reformer Gas Addition." DOI 10.1016/j.fuel.2006.08.011.
- [25] Wang, H., You, X., Joshi, A. V., Davis, S. G., Laskin, A., Egolfopoulos, F., and Law, C. K., 2007, "USC Mech Version II. High-Temperature Combustion Reaction Model of H2/CO/C1-C4 Compounds."
- [26] Zhou, C.-W., Li, Y., Burke, U., Banyon, C., Somers, K. P., Ding, S., Khan, S., Hargis, J. W., Sikes, T., Mathieu, O., Petersen, E. L., AlAbbad, M., Farooq, A., Pan, Y., Zhang, Y., Huang, Z., Lopez, J., Loparo, Z., Vasu, S. S., and Curran, H. J., 2018, "An Experimental and Chemical Kinetic Modeling Study of 1,3-Butadiene Combustion: Ignition Delay Time and Laminar Flame Speed Measurements," Combust. Flame, 197, pp. 423–438. DOI https://doi.org/10.1016/j.combustflame.2018.08.006.
- [27] Smith, G. P., Golden, D. M., Frenklach, M., Moriarty, N. W., Eiteneer, B., Goldenberg, M., Bowman, C. T., Hanson, R. K., Song, S., Gardiner, W. C., Lissianski, V. V., and Qin, Z., "GRI-Mech 3.0" [Online]. Available: http://www.me.berkeley.edu/gri\_mech/. [Accessed: 02-Jan-2022].
- [28] Yang, X., Shen, X., Santer, J., Zhao, H., and Ju, Y., 2017, "HP Mechanism" [Online]. Available: http://engine.princeton.edu/mechanism/HP-Mech.html. [Accessed: 02-Jan-2022].